



Pre-chirp managed self-phase modulation for efficient generation of wavelength-tunable energetic femtosecond pulses

RUNZHI CHEN^{1,2} AND GUOQING CHANG^{1,2,*}

¹Beijing National Laboratory for Condensed Matter Physics, Institute of Physics, Chinese Academy of Sciences, Beijing 100190, China

²University of Chinese Academy of Sciences, Beijing 100049, China

*Corresponding author: guoqing.chang@iphy.ac.cn

Received 15 April 2020; revised 24 June 2020; accepted 1 July 2020; posted 2 July 2020 (Doc. ID 395275); published 28 July 2020

Self-phase-modulation-enabled spectral selection (SESS) allows generation of widely tunable femtosecond pulses. We propose pre-chirp managed SESS, in which the excitation pulse is properly pre-chirped to control the fiber-optic nonlinear spectral broadening and hence generate separated spectral lobes—a feature demanded by SESS. Besides offering improved efficiency compared with conventional energy-tuned SESS, this new method is able to reshape an input pulse of unwanted shape into a bell-shaped pulse that is desired for implementing SESS. The excellent energy scalability of pre-chirp managed SESS can produce megawatt-level femtosecond pulses widely tunable in the wavelength range of 0.86–1.3 μm . Such a powerful source is well suited to drive multiphoton microscopy to achieve deep-tissue imaging. © 2020 Optical Society of America

<https://doi.org/10.1364/JOSAB.395275>

1. INTRODUCTION

Many applications demand high-energy and wavelength-tunable femtosecond pulses. Due to the limited bandwidth of most laser materials, these energetic tunable pulses are normally derived from an ultrafast laser source via nonlinear wavelength conversion. The recent advance of ultrafast fiber lasers has spurred intensive research effort toward achieving wavelength conversion based on fiber-optic methods, such as supercontinuum generation [1,2], dispersive wave generation [3–6], fiber optical parametric oscillators/amplifiers [7–9], and soliton self-frequency shift [10–13], to name a few. Recently we proposed and demonstrated a new fiber-optic wavelength conversion method that features a broad tuning range, excellent energy scalability, and low timing jitter. Figure 1 illustrates a typical implementation based on a fiber laser system configured as master oscillator power amplifier (MOPA). A fiber oscillator emits weak seeding pulses that are amplified by a fiber amplifier, then compressed by a pair of diffraction gratings, and finally coupled into a short piece of optical fiber. By minimizing the effect of group-velocity dispersion (GVD), we can ensure that self-phase modulation (SPM) dominates the spectrum broadening such that the broadened spectrum features several well-separated spectral lobes. At the fiber output, we use suitable optical filters to select the leftmost/rightmost spectral lobes, which produces nearly transform-limited femtosecond pulses. This method is dubbed SPM-enabled spectral selection (SESS). We have demonstrated that SESS offers >400 nm wavelength

tuning range [14,15], produces ~ 100 fs pulses with >100 nJ energy corresponding to >1 MW peak power, and introduces relative timing jitter as low as ~ 0.1 fs [16,17]. The resulting fiber-laser-based SESS sources were applied to multiphoton microscopy imaging [18,19] and generation of high-power longwave mid-infrared pulses [20].

In all the current implementations, wavelength tuning was achieved by varying the coupled pulse energy into the fiber: more input-pulse energy leads to stronger spectral broadening, and the leftmost/rightmost spectral lobes shift further away from the center wavelength. However, this wavelength tuning method has the following drawbacks:

- (1) The full power capacity of the MOPA system is not efficiently used, as we reduce the coupled energy into the SESS fiber to shift the leftmost/rightmost spectral lobes closer to the center wavelength.
- (2) To achieve a wide wavelength tuning range and high conversion efficiency, bell-shaped pulses are preferred to drive SESS. However, in a real fiber MOPA system, the generated pulses might deviate significantly from a bell-shaped profile, and thus SPM-dominated spectral broadening is compromised, leading to inefficient SESS. Variation of the coupled pulse energy for wavelength tuning imposes no change to the pulse shape and therefore cannot improve the poor performance of SESS driven by excitation pulses with undesired shape.

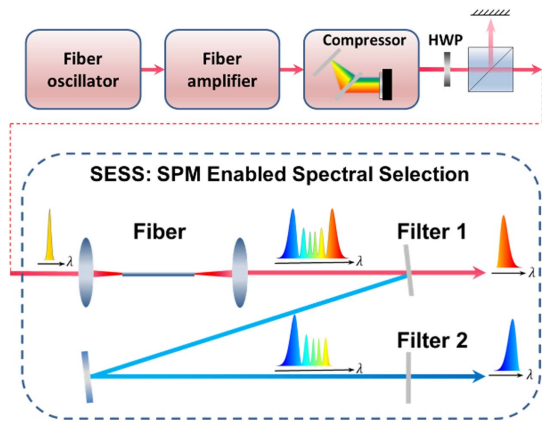


Fig. 1. Schematic of fiber-laser driven SESS source, which typically consists of four parts: a fiber oscillator that provides seeding pulses, a fiber amplifier that boosts the energy of seeding pulses, a diffraction-grating based compressor that de-chirps the amplified pulses, and a SESS device that produces wavelength-tunable energetic femtosecond pulses. Another crucial function of the compressor—as we demonstrate in this paper—is to flexibly pre-chirp the pulse used for driving SESS.

In this paper, we propose pre-chirp managed SESS to overcome these two drawbacks. In this method, we achieve wavelength tuning by pre-chirping the excitation pulses while fixing the pulse energy at the maximum value. A detailed numerical investigation shows that pre-chirping a pulse modifies its profile such that the performance of SESS can be significantly improved. A combination of high-power fiber laser technology and pre-chirp managed SESS allows generation of widely tunable pulses with ~ 1 MW peak power.

2. NUMERICAL MODEL FOR SESS

Propagation of femtosecond pulses inside an optical fiber can be accurately modeled by the generalized nonlinear Schrödinger equation (GNLSE) [21]:

$$\frac{\partial A(z, T)}{\partial z} + \left(\sum_{n \geq 2} \beta_n \frac{i^{n-1}}{n!} \frac{\partial^n}{\partial T^n} \right) A(z, T) = i\gamma \left(1 + \frac{i}{\omega_0} \frac{\partial}{\partial T} \right) \times \left(A(z, T) \int_{-\infty}^{+\infty} R(t') |A(z, T-t')|^2 dt' \right), \quad (1)$$

where $A(z, T)$ represents the amplitude envelope of the pulse. β_n denotes the n th-order fiber dispersion. γ is the nonlinear parameter defined as $\gamma = \omega_0 n_2 / (c A_{\text{eff}})$, where ω_0 is the center frequency, n_2 is the nonlinear-index coefficient, c the light speed in a vacuum, and A_{eff} is the mode-field area. For fused silica, n_2 has a typical value of $2.6 \times 10^{-20} \text{ m}^2/\text{W}$. $R(t)$ includes both the instantaneous electronic and delayed molecular responses (i.e., stimulated Raman scattering) of fused silica, and is normally given by

$$R(t) = (1 - f_R) \delta(t) + f_R \frac{\tau_1^2 + \tau_2^2}{\tau_1 \tau_2} \exp\left(\frac{-t}{\tau_2}\right) \sin\left(\frac{t}{\tau_1}\right), \quad (2)$$

where f_R , τ_1 , and τ_2 take typical values of 0.18, 12.2 fs, and 32 fs, respectively [21]. Selection of the leftmost/rightmost

spectral lobes by optical filtering is modeled in the spectral domain.

3. CONCEPT OF PRE-CHIRP MANAGED SESS: TAKE GAUSSIAN PULSE AS INPUT

To illustrate the general idea, we assume that the MOPA system is based on Yb-fiber laser technology and can deliver 200 fs (full width at half maximum, FWHM) transform-limited Gaussian pulse centered at $1.03 \mu\text{m}$. The fiber used in the simulation is a commercially available fiber (noted as LMA8), which has a mode-field diameter of $7.3 \mu\text{m}$; its dispersion curve is plotted in Fig. 2(a). In the simulation, the fiber length is set at 2.3 cm, and the maximum pulse energy in the fiber is 150 nJ. Figure 2(b) shows the spectral broadening as we increase the pulse energy into the fiber. Due to the use of short fiber, SPM dominates the spectral broadening, and consequently the broadened spectrum comprises separated spectral lobes. As we increase the input pulse energy from 60 to 150 nJ, the resulting spectrum becomes much broader, with the leftmost spectral lobe peaking at $0.89 \mu\text{m}$ and the rightmost one at $1.2 \mu\text{m}$. Using proper optical filters to select the leftmost/rightmost spectral lobes results in nearly transform-limited pulses. The simulation results in Fig. 2(b) suggest that the center wavelength of a SESS source can be tuned by varying the input pulse energy.

We filter the leftmost and rightmost spectral lobes [marked by dashed white lines in Fig. 2(b)] in the spectrum and calculate the corresponding pulse energy and duration as a function of the peak wavelength. The simulation results are summarized in Fig. 3. As the peak wavelength moves away from $1.03 \mu\text{m}$, the pulse energy increases while the pulse duration decreases. For the leftmost spectral lobes, the pulse energy drops from 24.7 to 15.1 nJ and the pulse duration increases from 46 to 70 fs as the peak wavelength of the SESS pulse is tuned from 0.89 to $0.96 \mu\text{m}$. For the filtered pulse corresponding to the rightmost spectral lobe, the pulse energy grows from 17.8 to 31.5 nJ and the duration decreases from 72 to 60 fs as the peak wavelength varies from 1.1 to $1.2 \mu\text{m}$.

To date, this wavelength tuning method (i.e., varying the input pulse energy) has been used for all the demonstrated SESS

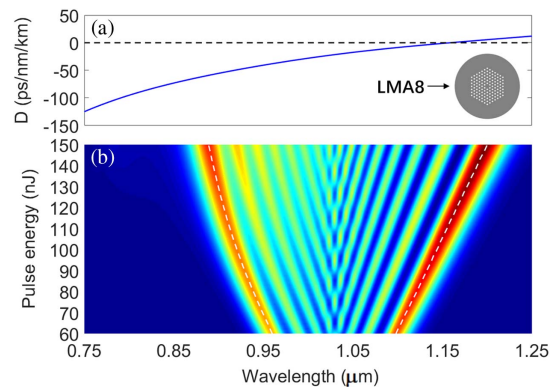


Fig. 2. Propagation of a 200 fs transform-limited Gaussian pulse through a 2.3 cm LMA-8 fiber. (a) Dispersion curve of the LMA-8 fiber. (b) Simulation results of the spectral broadening for different input pulse energy tuned from 60 to 150 nJ. Dashed white lines in (b) mark the leftmost and rightmost spectral lobes that are selected by suitable optical filters to generate femtosecond pulses.

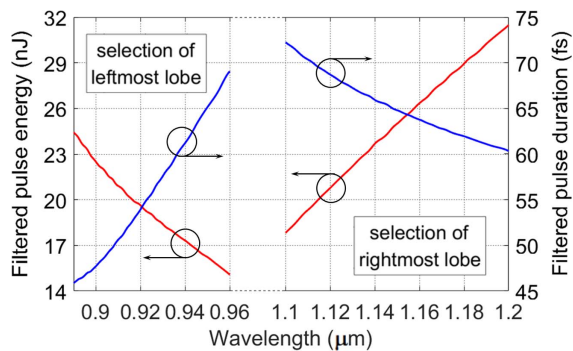


Fig. 3. Pulse energy (red curves) and duration (blue curves) versus corresponding center wavelength for filtering the outermost lobes of the spectra shown in Fig. 2(b).

sources [14–17]. In the following, we refer to this method as energy-tuned SESS. However, this method has an obvious drawback: it does not efficiently use the full energy capacity (i.e., 150 nJ) provided by the excitation source. For SESS driven by a fiber laser MOPA system, a pair of diffraction gratings (see Fig. 1) is normally employed to compress the amplified pulses before they are coupled into the short fiber to excite SESS. Such a configuration offers an alternative wavelength tuning method: adjust the grating separation to pre-chirp the excitation pulse coupled into the SESS fiber while maintaining the coupled pulse energy at 150 nJ. Varying the pre-chirp directly changes the duration of the excitation pulse and therefore controls the amount of nonlinear phase shift (NPS). As a result, the peak wavelength of the leftmost/rightmost spectral lobes can be tuned by managing the pre-chirp of the excitation pulse.

Figure 4 shows the broadened spectrum as we pre-chirp the input pulse by varying the group-delay dispersion (GDD) added to the optical spectrum of the initial unchirped Gaussian pulse. The pre-chirping GDD varies between $-20,000 \text{ fs}^2$ and $20,000 \text{ fs}^2$ with the excitation pulse energy fixed at 150 nJ. The broadened spectrum has the largest bandwidth corresponding to the unchirped excitation pulse; introducing pre-chirp, whether negative or positive, leads to a narrower spectrum as expected. Fortunately, during variation of the pre-chirping GDD, the spectrum maintains the feature of separated spectral lobes, which ensures the convenient selection of the leftmost/rightmost ones with high conversion efficiency.

Compared with wavelength tuning by adjusting excitation pulse energy, pre-chirp managed SESS generates more energetic wavelength-tunable femtosecond pulses. Figure 5 plots the energy (red curve) and duration (blue curve) of the SESS pulse by filtering the outermost spectral lobes. For the leftmost spectral lobes, the pulse energy rises from 24.7 to 32.7 nJ, and the pulse duration increases rapidly from 46 to 103 fs as the peak wavelength shifts from 0.89 to 0.96 μm . For the pulse corresponding to filtering the rightmost spectral lobe, the pulse energy drops from 39 to 31.5 nJ, and the pulse duration decreases from 106 to 60 fs as the peak wavelength shifts from 1.1 to 1.2 μm . A comparison between Fig. 3 and Fig. 5 shows that, as the peak wavelength shifts closer to the center wavelength of the excitation pulse, the SESS pulse energy decreases for energy-tuned SESS and increases for pre-chirp managed SESS while the SESS pulse duration increases for

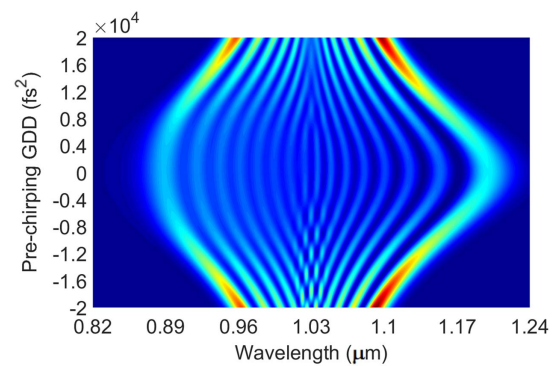


Fig. 4. Spectral broadening for pre-chirped Gaussian pulse propagating through 2.3 cm LMA-8 fiber. In the simulation, the pre-chirping GDD varies from $-20,000 \text{ fs}^2$ to $20,000 \text{ fs}^2$ while the pulse energy is fixed at 150 nJ.

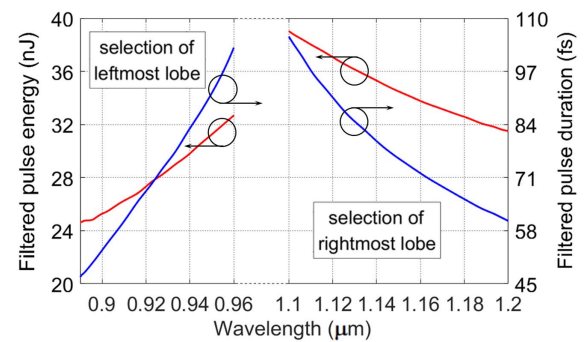


Fig. 5. Pulse energy (red curves) and duration (blue curves) versus center wavelength for filtering the outermost spectral lobes.

both methods. Especially for filtered pulses at the wavelength of 0.96 and 1.1 μm , the corresponding pulse energy achieved by pre-chirp managed SESS is more than doubled compared with that obtained by energy-tuned SESS.

Another intriguing feature in Fig. 4 is that the spectral broadening seems symmetric with respect to the sign of the pre-chirping GDD; that is, for the pre-chirping GDD (whether positive or negative) of the same magnitude, the resulting spectrum (especially for the outermost spectral lobes) appears nearly the same. To understand the mechanism, we plot in Fig. 6 the temporal and spectral evolution along the fiber length for the input excitation pulse with opposite pre-chirping GDDs of $20,000 \text{ fs}^2$ and $-20,000 \text{ fs}^2$. A comparison between Fig. 6(a) and Fig. 6(c) shows nearly identical evolution of the pulse in the time domain. Such a behavior arises from the fact that the fiber GVD plays a minimal role in the pulse propagation because nonlinearity (i.e., SPM and self-steepening) overtakes dispersion in such a short fiber. At the fiber input, the excitation pulses with opposite pre-chirping GDD have the same profile of $|A(T)|$ and opposite initial temporal phase. While SPM itself does not change the pulse profile, self-steepening reshapes the pulse such that the trailing edge of the pulse becomes steeper with the increased propagation distance. Interestingly, pulse reshaping due to self-steepening only depends on the initial pulse profile [21]. This explains why the two pulses with opposite initial phases develop nearly identical pulse profiles

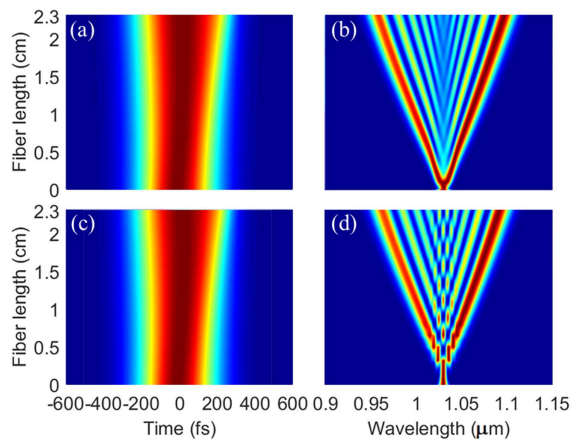


Fig. 6. [(a), (c)] Temporal and [(b), (d)] spectral evolution of 150 nJ chirped Gaussian pulses in 2.3 cm long LMA8 fiber. The Gaussian pulse at the fiber input of (a) and (b) is positively chirped by adding pre-chirping GDD of $20,000 \text{ fs}^2$, and the one for (c) and (d) is negatively chirped by adding pre-chirping GDD of $-20,000 \text{ fs}^2$.

evidenced by the results in Figs. 6(a) and 6(c). SPM and self-steepening exert NPS to the pulses as well. Compared with SPM, self-steepening plays a secondary role in the spectral broadening, and therefore the NPS acquired by the pulse mainly originates from SPM. Since SPM-caused NPS depends on the pulse profile rather than its initial phase, the two pulses shown in Figs. 6(a) and 6(c) obtain similar NPS. It is the combination of the initial phase and acquired NPS that determines the spectral evolution. For short fiber length (e.g., $z < 0.5 \text{ cm}$), NPS is small and the initial opposite phases of the two pulses result in different spectra: the spectrum corresponding to positive pre-chirping GDD is broadened [Fig. 6(b)], while the one corresponding negative pre-chirping GDD experiences narrowing first and then starts broadening afterwards [Fig. 6(d)]. For long fiber length (e.g., $z > 1.5 \text{ cm}$), NPS dominates the total phase and the two spectra become more similar to each other. Especially after propagation of 2.3 cm, the two spectra exhibit similar structure and bandwidth.

4. RESHAPING OF AIRY PULSE IN PRE-CHIRP MANAGED SESS

In a real fiber MOPA system, the generated pulses might deviate significantly from the bell-shaped profile due to uncompensated positive third-order dispersion (TOD), which leads to compressed pulses with a long oscillatory tail. In many numerical analyses, such a pulse shape is normally represented by an Airy pulse obtained by imposing a pure cubic phase on a Gaussian spectrum. In this section, we investigate the performance of SESS excited by an Airy pulse. In Section 3, the broadest spectrum is excited by the 150 nJ, 200 fs transform-limited Gaussian pulse corresponding to $\sim 700 \text{ kW}$ peak power (blue curve in Fig. 7). To have a fair comparison, we numerically generate the input Airy pulse by adding $2.5 \times 10^6 \text{ fs}^3$ TOD (i.e., pure cubic phase) to the spectrum of a 165 nJ, 140 fs transform-limited Gaussian pulse (red curve in Fig. 7). In this scenario, the resulting Airy pulse (black curve in Fig. 7) has a duration (FWHM) of 200 fs with 700 kW peak power. The resulting Airy pulse

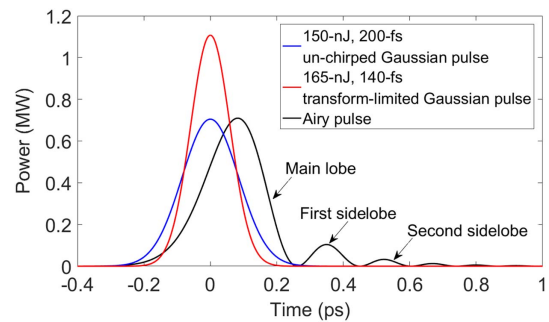


Fig. 7. Blue curve: 150 nJ, 200 fs unchirped Gaussian pulse used in Section 3. Black curve: Airy pulses that are obtained by adding $2.5 \times 10^6 \text{ fs}^3$ TOD to a 165 nJ, 140 fs transform-limited Gaussian pulse shown as the red curve.

features an asymmetric main lobe followed by an oscillatory tail consisting of numerous temporal lobes, which—as shown in Fig. 7—are termed the first sidelobe, the second sidelobe, and so on.

We then propagate the Airy pulse in 2.8 cm LMA fiber and plot the simulation results in Figs. 8(a), 8(d), and 8(g). Figure 8(d) shows the spectral broadening along the fiber length. As the fiber length is below 1.5 cm, the spectrum broadens and forms separated spectral lobes. The spectral lobes on the short-wavelength side starts to wash out due to increased positive GVD at the short-wavelength side [15]. Surprisingly, further propagation results in a clear powerful spectral lobe that gradually emerges at the short-wavelength side. The broadened spectrum at the 2.8 cm fiber length and the corresponding pulse are shown in Fig. 8(g) and Fig. 8(a), respectively. The output pulse [red curve in Fig. 8(a)] develops rapid oscillations at the trailing edge. A comparison between the output pulse and the

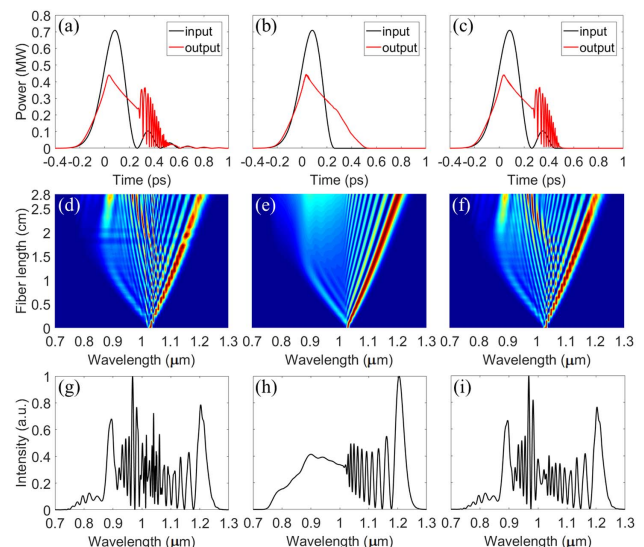


Fig. 8. Spectral broadening in 2.8 cm LMA-8 fiber with different input pulses: Airy pulse [black curve in (a)], the main lobe of the Airy pulse [black curve in (b)], and the main lobe together with the first sidelobe of the Airy pulse [black curve in (c)]. (d)–(f) The spectral evolution corresponding to the input pulses shown in (a)–(c), respectively. The spectra after 2.8 cm propagation are shown in (g)–(i), and their corresponding pulses are plotted as the red curves in (a)–(c).

input pulse [black curve in Fig. 8(a)] shows that the oscillation region overlaps with the entire first sidelobe and part of the second sidelobe.

To show the effect of these two sidelobes, we simulate the spectral evolution in 2.8 cm LMA8 excited by (i) the main lobe of the Airy pulse [black curve in Fig. 8(b)] and (ii) the main lobe together with the first sidelobe [black curve in Fig. 8(c)]. As Fig. 8(e) shows, for the propagation distance below 1.5 cm, the spectral evolution excited by the main lobe is similar to that excited by the Airy pulse. However, substantial difference occurs for further propagation: the short-wavelength side of the spectrum in Fig. 8(e) becomes spectrally flat and the separated spectral lobes developed at earlier stage disappear. This is evidently manifested by the spectrum after 2.8 cm propagation [Fig. 8(h)]. The red curve in Fig. 8(b) shows the corresponding pulse, which has an elongated trailing edge extending up to ~ 400 fs away from the peak of the input main lobe. The trailing edge monotonically drops as it moves away from the peak without any rapid oscillations.

As we use the main lobe together with the first sidelobe as the input, the spectral evolution [Fig. 8(f)] is almost identical with that [Fig. 8(d)] corresponding to the Airy pulse. The spectrum after 2.8 cm propagation [Fig. 8(i)] develops an isolated spectral lobe peaking at $0.9 \mu\text{m}$; accordingly, the corresponding pulse [red curve in Fig. 8(c)] forms rapid oscillations at its trailing edge.

Above simulations demonstrate that the first sidelobe of the Airy pulse plays an important role in the development of fine spectral structures. The sidelobe causes temporal rapid oscillation when the main lobe develops an elongated trailing edge, which thus renders formation of spectral lobes at the short-wavelength side of the broadened spectrum. The spectral lobe at $0.9 \mu\text{m}$ can be filtered out producing 26.6 nJ, 64 fs pulses with a Strehl ratio of 74%.

We next investigate the performance of energy-tuned SESS excited by the Airy pulse. As Fig. 9(a) shows, decreasing the coupled pulse energy from 165 to 65 nJ substantially narrows the spectrum, and the rightmost spectral lobe shifts from 1.2 to $1.1 \mu\text{m}$. However, different from the results in Fig. 2(b) corresponding to Gaussian pulse as input, the leftmost spectral lobe gradually disappears with reduced pulse energy. This is clearly shown by the spectrum [red curve in Fig. 9(b)], as the input Airy pulse has an energy of 65 nJ. The red curve in Fig. 9(c) plots the corresponding pulse. We also plot in Figs. 9(b) and 9(c) the results when we use the main lobe (black curves) and the main lobe together with the first sidelobe (blue dashed curves) of the 65 nJ Airy pulse as the excitation pulses. Clearly, as the pulse energy is reduced from 165 to 65 nJ, the main lobe has a less extended trailing edge, which results in oscillation at only the leading edge of the first sidelobe. Such oscillation leads to fine structures in the wavelength range of 0.96 – $1.05 \mu\text{m}$; the plateau below $0.96 \mu\text{m}$ is generated from the main lobe and nearly unaffected by the oscillation.

The results in Fig. 9 suggest that energy-tuned SESS excited by the Airy pulse fails to generate femtosecond pulses tunable at the short-wavelength side. This is mainly caused by the complicated interplay between the main lobe and the sidelobes during the nonlinear propagation of the Airy pulse. Fortunately,

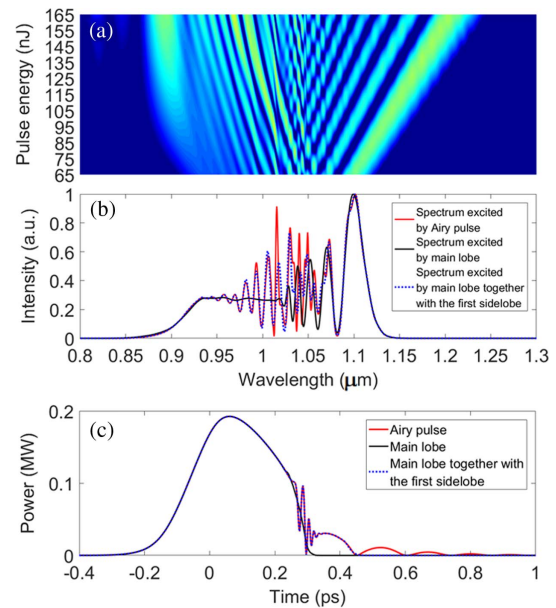


Fig. 9. Energy-tuned SESS for an Airy pulse in 2.8 cm LMA8 fiber. (a) Broadened spectra of an Airy pulse with the energy varying between 165 and 65 nJ. Results are shown in log scale with the same normalization as Fig. 11 for better comparison. (b) Broadened spectra and (c) their corresponding pulses obtained from propagation of 65 nJ Airy pulse (red curves), the main lobe (black curves), and the main lobe together with the first sidelobe (blue dashed curves).

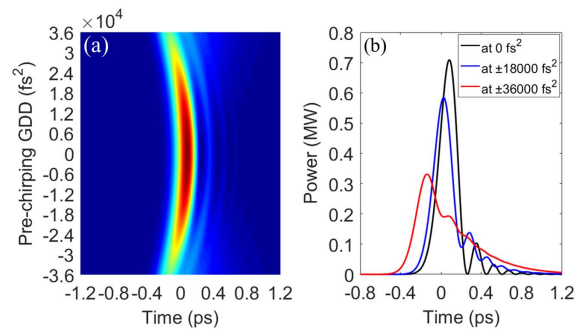


Fig. 10. (a) Pre-chirping the Airy pulse by varying the pre-chirping GDD from $-36,000$ to $36,000 \text{ fs}^2$. (b) Initial Airy pulse (black curve) and two chirped pulses corresponding to the pre-chirping GDD at $\pm 18,000 \text{ fs}^2$ (blue curve) and $\pm 36,000 \text{ fs}^2$ (red curve).

pre-chirping the Airy pulse can stretch it, mitigate its oscillatory tail structures, and eventually eliminate the sidelobes. Figure 10(a) shows the variation of the pulse profile as we add different amount of pre-chirping GDD to the Airy pulse. As we increase the magnitude of pre-chirping GDD, the peak of the Airy pulse shifts towards the leading edge. Figure 10(b) shows two chirped pulses corresponding to a pre-chirping GDD of $\pm 18,000 \text{ fs}^2$ (blue curve) and $\pm 36,000 \text{ fs}^2$ (red curve); for a better comparison, the Airy pulse without pre-chirping is shown as the black curve. Clearly, with increased pre-chirping GDD, the sidelobes in the initial Airy pulse gradually disappear and evolve into a slowly decaying tail.

Figure 11 shows the broadened spectra in the 2.8 cm LMA8 fiber using the pre-chirped Airy pulses shown in Fig. 10(a). As

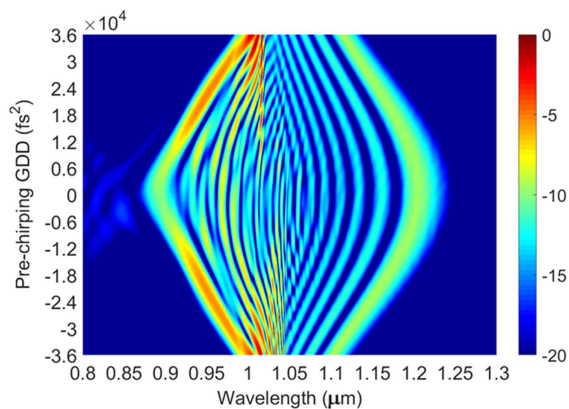


Fig. 11. Spectral broadening of chirped Airy pulse with the pre-chirping GDD varying from $-36,000$ to $36,000$ fs^2 . Results are shown in log scale.

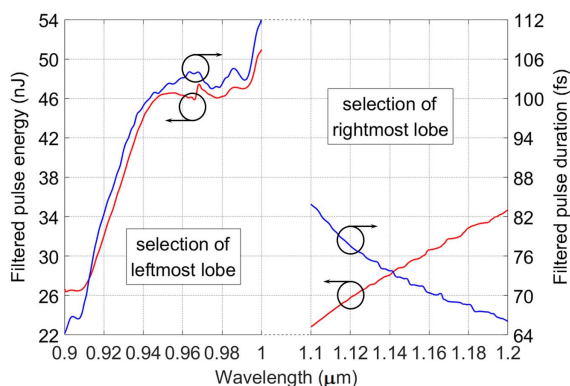


Fig. 12. Pulse energy (red curves) and duration (blue curves) versus wavelength resulting from selection of the outermost spectral lobes in Fig. 11 with the pre-chirping GDD varying from 0 to $-36,000$ fs^2 .

the magnitude of the pre-chirping GDD increases from 0 to $36,000$ fs^2 , the broadened spectra maintain the well-separated spectral lobes at both wavelength sides. Figure 12 presents the pulse energy and duration of the SESS pulses corresponding to the pre-chirping GDD varying from 0 to $-36,000$ fs^2 . The leftmost spectral lobes result in ultrashort pulses with the energy (duration) increasing from 26.6 nJ (64 fs) to 51 nJ (112 fs) as the peak wavelength shifts from 0.9 to 1 μm . As the peak wavelength of the rightmost spectral lobe shifts from 1.1 to 1.2 μm , the pulse energy increases from 22.8 to 34.7 nJ, while the duration decreases from 84 to 66 fs.

5. RESHAPING OF A FLAT-TOP PULSE IN PRE-CHIRP MANAGED SESS

As we have shown, SPM dominates the spectral broadening in SESS. SPM-caused NPS is proportional to $|A(T)|^2$, which introduces nonlinear chirp $\delta\omega(T) \propto \partial|A(T)|^2/\partial T$ and broadens the optical spectrum. The amount of spectral broadening is highly dependent on the pulse shape $|A(T)|^2$. The simulations in Section 3 suggest that Gaussian pulses are efficient in implementing SESS. Indeed, any bell-shaped pulses (e.g., hyperbolic secant, Lorentzian, etc.) are suitable candidates. Bell-shaped

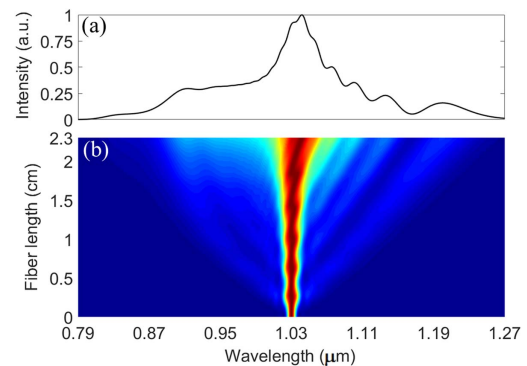


Fig. 13. Propagation of a 150 nJ, 340 fs unchirped super-Gaussian pulse ($m = 3$) through a 2.3 cm LMA-8 fiber. (a) Optical spectrum at the output of 2.3 cm fiber. (b) Spectral evolution with respect to fiber length.

pulses feature a rapid power drop as they move away from the pulse peak, which renders a large nonlinear chirp and facilitates SPM-dominated spectral broadening. Consequently, a considerable portion of pulse energy is transferred to the outermost spectral lobes. In contrast, the worst scenario occurs if the pulse has a flat top; that is, the central part of the pulse intensity profile varies slowly or, even worse, stays constant in time. This part contains a large portion of pulse energy but contributes little to the SPM-induced spectral broadening, which prevents efficient SESS.

Indeed, flat-top pulses are desired in certain applications including optical communication, frequency conversion, and optical switching. Since an ultrafast laser might not naturally deliver flat-top pulses, these pulses are normally obtained via pulse shaping techniques [22–24]. In numerical modeling of their propagation in an optical fiber, flat-top pulses are usually represented by super-Gaussian pulses [25–27]. In this section, we take super-Gaussian pulses as an example to show how the pulse shape affects SESS. An unchirped super-Gaussian pulse is written as $A(T) = \sqrt{P_0} \exp[-(T/T_0)^{2m}/2]$, where m denotes the order of the super-Gaussian pulse. In the following simulation, we assume that the input is a third-order super-Gaussian pulse (i.e., $m = 3$) and $T_0 = 181$ fs (corresponding to FWHM of 340 fs) such that this pulse has the same initial spectral width as the Gaussian pulse in Section 3. Figure 13 shows the spectral broadening for the unchirped super-Gaussian pulse with 150 nJ pulse energy propagating in fiber LMA8. Distinctly different from Gaussian-pulse-driven spectral broadening as shown in Fig. 2(b), the central part of the input spectrum experiences much less broadening but contains a large portion of energy. The broadened spectrum develops long shallow leading and trailing edges without forming separated spectral lobes, making it unsuitable for implementing efficient SESS.

To solve this issue caused by the undesired pulse shape, the pulse should be transformed into a bell shape before being coupled into the fiber. Fortunately, such a transformation can be achieved in pre-chirp managed SESS. Figure 14(a) shows the variation of the resulting pulse profile as we add different amounts of pre-chirping GDD to the optical spectrum of the third-order unchirped super-Gaussian pulse. As we increase the magnitude of pre-chirping GDD, the pulse becomes shorter

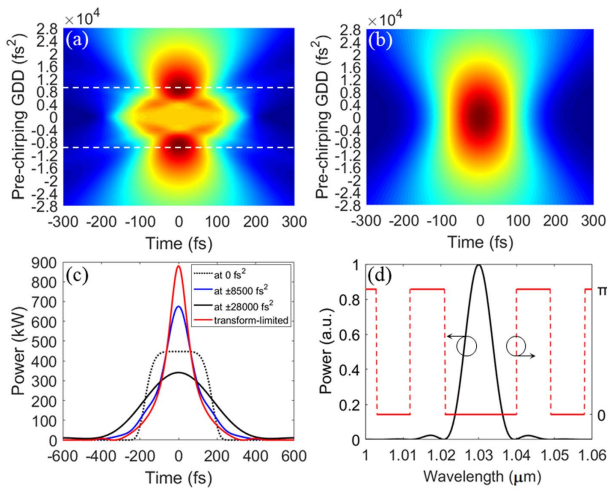


Fig. 14. Pulse evolution as a function of added pre-chirping GDD to the spectrum of different unchirped pulses: (a) super-Gaussian pulse ($m = 3$) and (b) Gaussian pulse. (c) Transformation of unchirped super-Gaussian pulse (dotted black curve) into bell-shaped pulses by adding pre-chirping GDD. Solid blue curve and black curve represent the chirped pulses corresponding to pre-chirping GDD of $\pm 8500 \text{ fs}^2$ and $\pm 28,000 \text{ fs}^2$, respectively. The transform-limited pulse given by the optical spectrum is shown as the red curve. (d) Optical spectrum of the unchirped super-Gaussian pulse (black curve) and the spectral phase (red curve). In (a), the pulse reaches the shortest duration (FWHM) of 169 fs for the pre-chirping GDD at 8500 fs^2 or -8500 fs^2 marked by the dashed white lines.

first and then stretches to longer duration. The pulse reaches the shortest duration of 169 fs for the pre-chirping GDD at 8500 fs^2 or -8500 fs^2 , marked by the dashed white lines in Fig. 14(a). Such a variation clearly differs from the case corresponding to a Gaussian pulse. As Fig. 14(b) shows, adding GDD to the optical spectrum of a transform-limited Gaussian pulse always elongates the unchirped pulse, and the resulting chirped pulse maintains a Gaussian profile. In contrast, pre-chirping an unchirped super-Gaussian pulse leads to a chirped pulse that substantially deviates from super-Gaussian profile.

To make a straightforward comparison, we plot in Fig. 14(c) the unchirped super-Gaussian pulse (dotted black curve), and two chirped pulses corresponding to a pre-chirping GDD of $\pm 8500 \text{ fs}^2$ (blue curve) and $\pm 28,000 \text{ fs}^2$ (solid black curve). These two chirped pulses exhibit a bell-shaped profile, and the former is shorter than the initial unchirped super-Gaussian pulse. The transform-limited pulse given by the optical spectrum of the unchirped super-Gaussian pulse is plotted in Fig. 14(c) as the red curve. Apparently, unlike an unchirped Gaussian pulse—which is also a transform-limited pulse, unchirped super-Gaussian pulse is *not* transform limited. This is because, as shown in Fig. 14(d), the optical spectrum (black curve) of the unchirped super-Gaussian pulse has a discontinuous phase that jumps between 0 and π (red curve). When the pre-chirp is introduced, the spectral components in phase (i.e., without relative phase differences) tend to lose their constructive interferences and stretch the pulse; the out-of-phase (i.e., with π phase difference) spectral components tend to lose their destructive interferences and shorten the pulse. As the

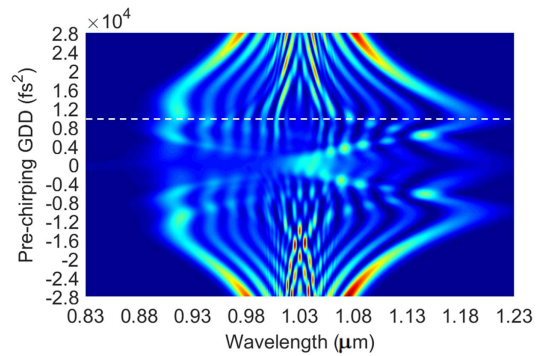


Fig. 15. Pre-chirp managed spectral broadening in 2.3 cm LMA-8 fiber. The input pulses are obtained by adding pre-chirping GDD to the optical spectrum of the unchirped super-Gaussian pulse ($m = 3$) with 150 nJ pulse energy. Simulation results of the spectral broadening for introduced GDD tuned from $-28,000$ to $28,000 \text{ fs}^2$. Dashed white lines mark the pre-chirping GDD of $10,000 \text{ fs}^2$.

magnitude of pre-chirping GDD is less than 8500 fs^2 , the shortening effect is dominant, and consequently the super-Gaussian pulse becomes compressed and reshaped. As we further increase the magnitude from 8500 fs^2 to $28,000 \text{ fs}^2$, the stretching overtakes the shortening and the chirped pulse becomes longer while maintaining the bell-shaped profile.

The results in Fig. 14 immediately suggest that pre-chirping an unchirped super-Gaussian pulse into a bell-shaped pulse can facilitate SPM-dominated spectral broadening to form separated spectral lobes—a feature desired by SESS. To confirm this speculation, we carry out simulation in which those pulses shown in Fig. 14(a) are taken as input to propagate in 2.3 cm fiber LMA8. During the simulation, the pulse energy is fixed at 150 nJ. Figure 15 shows the broadened spectra at the fiber output. As the magnitude of the pre-chirping GDD exceeds $10,000 \text{ fs}^2$ (marked by a dashed white line), the broadened spectrum develops well-separated spectral lobes with a considerable portion of energy contained by the leftmost/rightmost lobes.

To show that pre-chirping a flat-top pulse can enable SESS, we filter the leftmost/rightmost spectral lobes of the spectra that correspond to pre-chirping GDD varying from $10,000$ to $28,000 \text{ fs}^2$. As Fig. 16 shows, selection of the leftmost spectral lobes results in ultrashort pulses whose energy (duration) increases from 27.2 nJ (66 fs) to 34.4 nJ (130 fs) as the peak wavelength shifts from 0.92 to $0.98 \mu\text{m}$. For the selection of

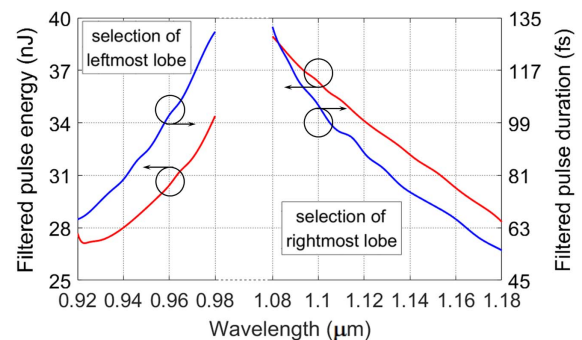


Fig. 16. Pulse energy (red curves) and duration (blue curves) versus wavelength resulting from selection of the outermost spectral lobes in Fig. 15 with the pre-chirping GDD varying from $10,000$ to $28,000 \text{ fs}^2$.

the rightmost spectral lobes, the pulse energy (duration) drops from 38.9 nJ (132 fs) to 28.3 nJ (55 fs) as the peak wavelength shifts from 1.08 to 1.18 μm . A comparison between Fig. 16 and Fig. 5 shows that the results corresponding to the pre-chirping the super-Gaussian pulses are similar (in terms of pulse energy and duration) to those obtained by pre-chirping the Gaussian pulse.

6. PRE-CHIRP MANAGED SESS FOR ACHIEVING TUNABLE PULSES AT MEGAWATT-LEVEL PEAK POWER

Yb-fiber lasers exhibit excellent power/energy scalability. Construction of an Yb-fiber MOPA based on chirped-pulse amplification with ~ 1 μJ pulse energy is relatively straightforward. Such a laser capability allows us to investigate the energy scalability of pre-chirp managed SESS. We carry out another set of simulations, in which the input pulses are obtained by adding pre-chirping GDD to the optical spectrum of an unchirped 200 fs Gaussian pulse.

Figure 17(a) illustrates the spectral evolution of the 500 nJ chirped Gaussian pulses propagating in 2.3 cm LMA8 fiber as the magnitude of the added pre-chirping GDD varies between 0 and 40,000 fs^2 . For pre-chirping GDD at 0, the resulting spectrum from 500 nJ unchirped Gaussian pulse is substantially broader than the spectrum obtained from 150 nJ unchirped Gaussian pulse. Due to much stronger nonlinearity, optical wave breaking associated with positive GVD appears manifesting as the spectral pedestal at the short-wavelength side. Fortunately, adding more GDD strongly pre-chirps the input pulse, which mitigates the effect of GVD, suppresses optical wave breaking, and thus ensures SPM-dominated spectral broadening. For example, as we increase the pre-chirping GDD to 16,000 fs^2 [marked by the dashed white line in Fig. 17(a)], the resulting spectrum recovers the structure of separated spectral lobes. For further increasing the pre-chirping GDD, such a desired spectral structure maintains and the outermost spectral lobes shift towards the center wavelength of the input pulse. Another benefit brought by pre-chirping the input pulse is that the pulse peak power is reduced to mitigate the possible surface damage to the fiber ends. In experiments, endcaps can be spliced to both the input and output ends to further ensure damage-free operation.

Figure 17(b) shows the energy (red curve) and duration (blue curve) of the SESS pulse by filtering the outermost spectral lobes. Compared with the results in Fig. 5 corresponding to 150 nJ excitation pulses, increasing the pulse energy of the chirped Gaussian pulse from 150 to 500 nJ improves the SESS pulse energy by a factor of about 3. More importantly, the wavelength tuning range increases from 0.89–1.2 μm to 0.86–1.3 μm . It is worth noting that 1.3 μm corresponds to one of the biological transmission windows [28]. Femtosecond pulses at this wavelength are identified as the best choice for driving multiphoton microscopy to achieve deep-tissue imaging [29]. The results in Fig. 17(b) show that our pre-chirp managed SESS source can deliver 80 fs pulses with 91.4 nJ energy at 1.3 μm ; the peak power is as high as 1.14 MW. Such SESS pulses of megawatt (MW) peak power constitute a desirable driving

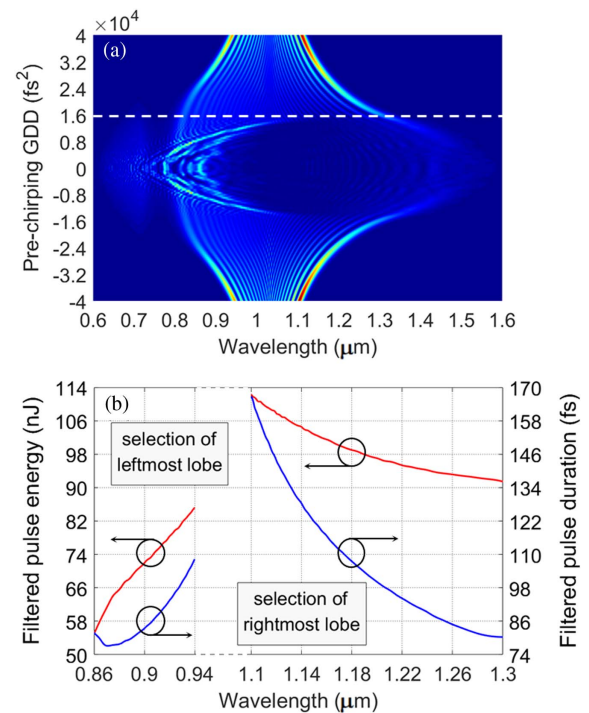


Fig. 17. Pre-chirp managed SESS in 2.3 cm LMA-8 fiber excited by chirped Gaussian pulses with 500 nJ energy. (a) Pre-chirp managed spectral broadening; (b) energy (red curve) and duration (blue curve) of the SESS pulse by filtering the outermost spectral lobes.

source for three-photon excited microscopy for biomedical imaging [30].

7. CONCLUSION

To conclude, we propose pre-chirp managed SESS, which outperforms current energy-tuned SESS. It is noteworthy that pre-chirping the input pulse into an optical fiber to control its nonlinear propagation is a powerful technique, which has been applied to nonlinear fiber amplifiers [31,32], femtosecond pulse delivery [33–35], nonlinear pulse compression [36–38], and control of dispersive wave generation [3] and soliton self-frequency shift [39]. Our work here—to the best of our knowledge—demonstrates for the first time that this technique can be employed to control SPM-dominated spectral broadening to facilitate SESS and achieve energetic tunable pulses. Besides more efficient use of laser pulse energy, pre-chirp managed SESS can modify input pulses of unwanted shapes (e.g., Airy pulse and flat-top pulse) into a bell-shaped pulse and therefore substantially improve the SESS performance. In other words, to efficiently excite energy-tuned SESS, the MOPA system has to deliver high-quality bell-shaped pulses. In contrast, pre-chirp managed SESS removes this requirement on the pulse shape, making it easier to construct the MOPA system. The required pre-chirping GDD is at the order of tens of thousands of fs^2 , which corresponds to variation of the grating-pair separation by about 1 cm. Such a small tuning can be easily implemented in the MOPA system without adding complexity or compromising compactness. We also show that pre-chirp managed SESS exhibits excellent energy scalability. Using 1 μJ

level Yb-fiber laser as the excitation source, pre-chirp managed SESS can generate MW-level femtosecond pulses widely tunable between 0.86–1.3 μm . Such an energetic ultrafast source is of particular interest for multiphoton microscopy aiming for deep-tissue imaging.

Funding. Guangdong Key RD Program (2018B090904003); National Natural Science Foundation of China (11774234); Chinese Academy of Sciences (YJKYYQ20190034).

Acknowledgment. We thank Prof. Zhiyi Wei of Institute of Physics CAS for useful discussions.

Disclosures. The authors declare no conflicts of interest.

REFERENCES

1. Y. Liu, H. Tu, W. A. Benalcazar, E. J. Chaney, and S. A. Boppart, "Multimodal nonlinear microscopy by shaping a fiber supercontinuum from 900 to 1160 nm," *IEEE J. Sel. Top. Quantum Electron.* **18**, 1209–1214 (2012).
2. H. Tu, Y. Liu, D. Turchinovich, M. Marjanovic, J. K. Lyngsø, J. Lægsgaard, E. J. Chaney, Y. Zhao, S. You, W. L. Wilson, B. Xu, M. Dantus, and S. A. Boppart, "Stain-free histopathology by programmable supercontinuum pulses," *Nat. Photonics* **10**, 534–540 (2016).
3. F. Tauser, F. Adler, and A. Leitenstorfer, "Widely tunable sub-30-fs pulses from a compact erbium-doped fiber source," *Opt. Lett.* **29**, 516–518 (2004).
4. G. Q. Chang, L.-J. Chen, and F. X. Kaertner, "Highly efficient Cherenkov radiation in photonic crystal fibers for broadband visible wavelength generation," *Opt. Lett.* **35**, 2361–2363 (2010).
5. H. Tu, J. Laegsgaard, R. Zhang, S. Tong, Y. Liu, and S. A. Boppart, "Bright broadband coherent fiber sources emitting strongly blue-shifted resonant dispersive wave pulses," *Opt. Express* **21**, 23188–23196 (2013).
6. K.-C. Li, L. H. Huang, J.-H. Liang, and M.-C. Chan, "Simple approach to three-color two-photon microscopy by a fiber-optic wavelength converter," *Biomed. Opt. Express* **7**, 4803–4815 (2016).
7. T. Gottschall, T. Meyer, M. Schmitt, J. Popp, J. Limpert, and A. Tünnermann, "Four-wave-mixing-based optical parametric oscillator delivering energetic, tunable, chirped femtosecond pulses for non-linear biomedical applications," *Opt. Express* **23**, 23968–23977 (2015).
8. K. Yang, J. Jiang, Z. Guo, Q. Hao, and H. Zeng, "Tunable femtosecond laser from 965 to 1025 nm in fiber optical parametric oscillator," *IEEE Photon. Technol. Lett.* **30**, 607–610 (2018).
9. M. Brinkmann, A. Fast, T. Hellwig, I. Pence, C. L. Evans, and C. Fallnich, "Portable all-fiber dual-output widely tunable light source for coherent Raman imaging," *Biomed. Opt. Express* **10**, 4437–4449 (2019).
10. H. Lim, J. Buckley, A. Chong, and F. W. Wise, "Fibre-based source of femtosecond pulses tunable from 1.0 to 1.3 microns," *Electron. Lett.* **40**, 1523–1525 (2004).
11. K. Wang and C. Xu, "Tunable high-energy soliton pulse generation from a large-mode-area fiber and its application to third harmonic generation microscopy," *Appl. Phys. Lett.* **99**, 071112 (2011).
12. J. W. Nicholson, A. Desantolo, W. Kaenders, and A. Zach, "Self-frequency-shifted solitons in a polarization maintaining, very-large-mode area, Er-doped fiber amplifier," *Opt. Express* **24**, 23396–23402 (2016).
13. L. Rishøj, B. Tai, P. Kristensen, and S. Ramachandran, "Soliton self-mode conversion: revisiting Raman scattering of ultrashort pulses," *Optica* **6**, 304–308 (2019).
14. W. Liu, C. Li, Z. Zhang, F. X. Kaertner, and G. Q. Chang, "Self-phase modulation enabled, wavelength-tunable fiber laser sources: an energy scalable approach," *Opt. Express* **24**, 15319–15340 (2016).
15. H.-Y. Chung, W. Liu, Q. Cao, F. X. Kaertner, and G. Q. Chang, "Er-fiber laser based, energy scalable ultrafast sources tunable in 1300–1700 nm," *Opt. Express* **25**, 15760–15771 (2017).
16. H.-Y. Chung, W. Liu, Q. Cao, L. W. Song, F. X. Kaertner, and G. Q. Chang, "Megawatt peak power tunable femtosecond source based on self-phase modulation enabled spectral selection," *Opt. Express* **26**, 3684–3695 (2018).
17. Y. Hua, G. J. Zhou, W. Liu, X. Min, F. X. Kaertner, and G. Q. Chang, "Ultrafast two-color source synchronized at 100-as-level precision based on SPM-enabled spectral selection," *Opt. Lett.* **45**, 3410–3413 (2020).
18. H.-Y. Chung, R. Greinert, F. X. Kaertner, and G. Q. Chang, "Multimodal imaging platform for optical virtual skin biopsy enabled by a fiber-based two-color ultrafast source," *Biomed. Opt. Express* **10**, 514–525 (2019).
19. H.-Y. Chung, W. Liu, Q. Cao, R. Greinert, F. X. Kaertner, and G. Q. Chang, "Novel fiber-based ultrafast source tunable between 1.15 μm and 1.35 μm for harmonic generation microscopy in human skin," *IEEE J. Sel. Top. Quantum Electron.* **25**, 3600111 (2019).
20. G. J. Zhou, Q. Cao, F. X. Kaertner, and G. Q. Chang, "Energy scalable, offset-free ultrafast mid-IR source harnessing self-phase modulation spectral selection," *Opt. Lett.* **43**, 2953–2956 (2018).
21. G. P. Agrawal, *Nonlinear Fiber Optics*, 5th ed. (Elsevier, 2013).
22. P. Petropoulos, M. Ibsen, A. D. Ellis, and D. J. Richardson, "Rectangular pulse generation based on pulse reshaping using a superstructured fiber Bragg grating," *J. Lightwave Technol.* **19**, 746–752 (2001).
23. F. Parmigiani, P. Petropoulos, M. Ibsen, and D. J. Richardson, "All-optical pulse reshaping and retiming systems incorporating pulse shaping fiber Bragg grating," *J. Lightwave Technol.* **24**, 357–364 (2006).
24. Y. Park, M. Kulishov, R. Slavík, and J. Azaña, "Picosecond and sub-picosecond flat-top waveform generation using uniform long-period fiber gratings," *Opt. Express* **14**, 12670–12678 (2006).
25. J. Rothhardt, S. Hädrich, T. Gottschall, J. Limpert, A. Tünnermann, M. Rothhardt, M. Becker, S. Brückner, and H. Bartelt, "Generation of flat-top pump pulses for OPCPA by coherent pulse stacking with fiber Bragg gratings," *Opt. Express* **17**, 16332–16341 (2009).
26. G. P. Agrawal and M. J. Potasek, "Effect of frequency chirping on the performance of optical communication systems," *Opt. Lett.* **11**, 318–320 (1986).
27. D. Anderson and M. Lisak, "Propagation characteristics of frequency chirped super-Gaussian optical pulses," *Opt. Lett.* **11**, 569–571 (1986).
28. L. Shi, L. A. Sordillo, A. Rodriguez-Contreras, and R. Alfano, "Transmission in near-infrared optical windows for deep brain imaging," *J. Biophoton.* **9**, 38–43 (2016).
29. D. G. Ouzounov, T. Wang, M. Wang, D. D. Feng, N. G. Horton, J. C. Cruz-Hernández, Y.-T. Cheng, J. Reimer, A. S. Tolias, N. Nishimura, and C. Xu, "In vivo three-photon imaging of activity of GCaMP6-labeled neurons deep in intact mouse brain," *Nat. Methods* **14**, 388–390 (2017).
30. T. Wang, C. Wu, D. G. Ouzounov, W. Gu, F. Xia, M. Kim, X. Yang, M. R. Warden, and C. Xu, "In vivo Quantitative analysis of 1300-nm three-photon calcium imaging in the mouse brain," *eLife* **9**, e53205 (2020).
31. W. Liu, D. N. Schimpf, T. Eidam, J. Limpert, A. Tünnermann, F. X. Kaertner, and G. Q. Chang, "Pre-chirp managed nonlinear amplification in fibers delivering 100 W, 60 fs pulse," *Opt. Lett.* **40**, 151–154 (2015).
32. T. Heuermann, C. Gaida, M. Gebhardt, and J. Limpert, "Thulium-doped nonlinear fiber amplifier delivering 50 fs pulses at 20 W of average power," *Opt. Lett.* **43**, 4441–4444 (2018).
33. T. Le, G. Tempea, Z. Cheng, M. Hofer, and A. Stingl, "Routes to fiber delivery of ultra-short laser pulses in the 25 fs regime," *Opt. Lett.* **17**, 1240–1247 (2009).
34. M. Kalashyan, C. Lefort, L. Martínez-León, T. Mansuryan, L. Mouradian, and F. Louradour, "Ultrashort pulse fiber delivery with optimized dispersion control by reflection gratings at 800 nm," *Opt. Express* **20**, 25624–25635 (2012).
35. M. Andreana, T. Le, W. Drexler, and A. Unterhuber, "Ultrashort pulse Kagome hollow-core photonic crystal fiber delivery for nonlinear optical imaging," *Opt. Lett.* **44**, 1588–1591 (2019).

36. Z. Várallyay, J. Fekete, Á. Bányász, and R. Szipőcs, "Optimizing input and output chirps up to the third-order for sub-nanojoule, ultra-short pulse compression in small core area PCF," *Appl. Phys. B* **86**, 567 (2007).
37. I. Martial, D. Papadopoulos, M. Hanna, F. Druon, and P. Georges, "Nonlinear compression in a rod-type fiber for high energy ultrashort pulse generation," *Opt. Express* **17**, 11155–11160 (2009).
38. T. Ganz, V. Pervak, A. Apolonski, and P. Baum, "16 fs, 350 nJ pulses at 5 MHz repetition rate delivered by chirped pulse compression in fibers," *Opt. Lett.* **36**, 1107–1109 (2011).
39. Y. Rosenberg, J. Drori, D. Bermudez, and U. Leonhardt, "Boosting few-cycle soliton self-frequency shift using negative prechirp," *Opt. Express* **28**, 3107–3115 (2020).